

Self-Supervised Training with Autoencoders for Visual Anomaly Detection

Alexander Bauer

Abstract—Deep convolutional autoencoders provide an effective tool for learning non-linear dimensionality reduction in an unsupervised way. Recently, they have been used for the task of anomaly detection in the visual domain. By optimising for the reconstruction error using anomaly-free examples, the common belief is that a trained network will have difficulties to reconstruct anomalous parts during the test phase. This is usually done by controlling the capacity of the network by either reducing the size of the bottleneck layer or enforcing sparsity constraints on its activations. However, neither of these techniques does explicitly penalise reconstruction of anomalous signals often resulting in a poor detection. We tackle this problem by adapting a self-supervised learning regime which allows to use discriminative information during training while regularising the model to focus on the data manifold by means of a modified reconstruction error resulting in an accurate detection. Unlike related approaches, the inference of the proposed method during training and prediction is very efficient processing the whole input image in one single step. Our experiments on the MVTec Anomaly Detection dataset demonstrate high recognition and localisation performance of the proposed method. On the texture-subset, in particular, our approach consistently outperforms a bunch of recent anomaly detection methods by a big margin.

Index Terms—Anomaly detection, autoenoders, inpainting.

1 INTRODUCTION

THE task of anomaly detection in a broad sense corresponds to searching for patterns which considerably deviate from some concept of normality. What is normal and what is a deviation might be very subtle and strongly depends on the application. The existing detection algorithms [1], [2], [3], [4], [5], [6], [7], [8], [9], [10], [11] typically assume that we only have access to the normal data while the anomalous examples are very scarce and are usually used to tune the hyperparameters of a model. The prevalent direction of research was focusing on so-called one-class classifiers [1], [12] which aim at learning a tight decision boundary around the normal data and define a distance-based anomaly score relative to the center of the training data. The success of this approach depends on the availability of pre-trained features and usually allows for detection of outliers only which strongly deviate from the normal structure. In practice, however, we usually are interested in more subtle deviations which require a good representation of the data manifold. The same applies to the combined approach based on training deep neural networks directly with the one-class objective [2], [13], [14]. Although this objective forces the network to concentrate the training data in a small region in the feature space, there is no guarantee that anomalous examples unseen during training will be mapped to a different location outside of the decision boundary.

Recently, deep autoencoders have been used for the task of anomaly detection in the visual domain [3], [15], [16]. Unlike one-class based approaches, they additionally allow for locating the anomalous regions in images by leveraging

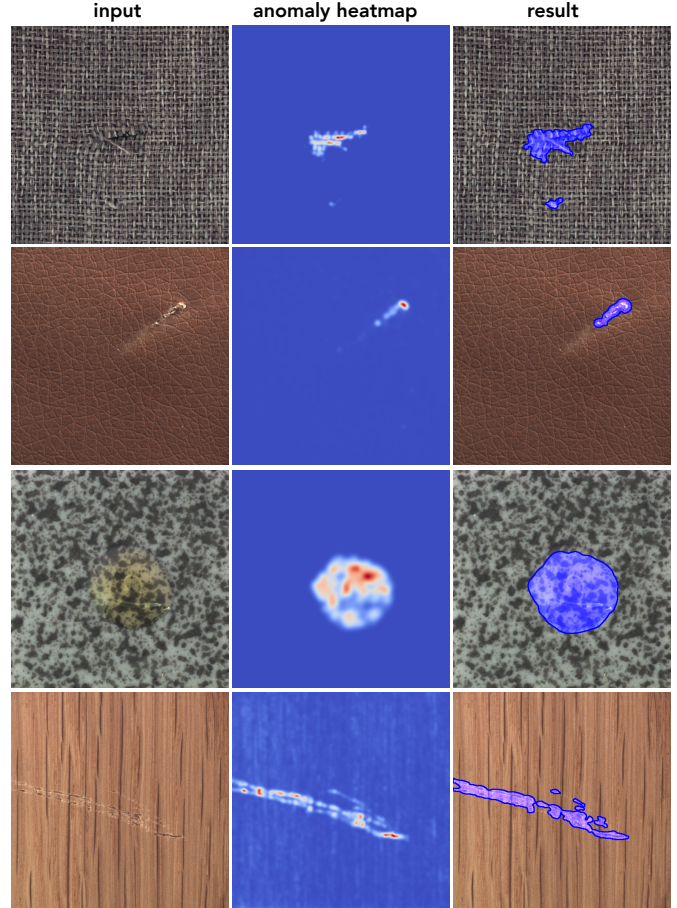


Fig. 1. Some anomaly detection results of our approach. Each row shows an input image, a corresponding anomaly heatmap and final detection result, respectively.

A. Bauer is an independent researcher. Previously he was with Berlin Big Data Center, and Machine Learning Group, Technische Universität Berlin Marchstr. 23, Berlin, Germany (e-mail: alexander.bauer@ki-architekt.com).

the pixel-wise nature of a corresponding training objective. By optimising for the reconstruction error using anomaly-free examples, the common belief is that after the training a corresponding network will have difficulties to reconstruct anomalous parts in the application phase. This is usually addressed by controlling the capacity of the network by either reducing the size of the bottleneck layer or enforcing sparsity constraints on the inner activations [17], [18]. However, neither of these techniques does explicitly penalise reconstruction of anomalous signals often resulting in a poor detection. This is similar to the issue related to training with the one-class objective, where no explicit mechanism exists for preventing anomalous points from being mapped to the normal region. In fact, a deep network optimised for the reconstruction error aims at compressing and reconstructing an input image and does not care much about the distinction between normal and anomalous pixels. As a result, the reconstruction errors for the anomalous and normal regions can be very similar preventing reliable detection.

In this paper, we propose a self-supervised learning framework which introduces discriminative information during training to prevent good reconstruction of anomalous patterns in the testing phase. We begin with an observation that the abnormality of a region in an image can be characterised by how well it can be reconstructed from the context of the surrounding pixels. Imagine an image where a small patch has been cut out by setting the corresponding pixel values to zeros. We can try to reconstruct this patch by extrapolating the surrounding pixel values according to our knowledge about the patch distribution of the training data. If the reconstruction strongly deviates from the original image, we consider a corresponding patch to be anomalous and normal otherwise. Following this intuition, we feed partially distorted images to the network during training while forcing it to reconstruct the original data similar to the task of neural image completion [19], [20], [21], [22], [23]. However, instead of setting individual pixels to zeros as for the completion task, we apply a transformation which approximately preserves the color distribution of the individual regions making it more difficult for the network to realise which image regions have been modified. In order to succeed the network now must learn features which are suitable for accomplishing two different tasks: a) detection of regions deviating from an expected pattern and b) reconstruction of such regions from the neighbouring pixel sets. Since this approach utilises no explicit information (e.g., label mask) about the location of the anomalous regions, it regularises the model to produce locally consistent reconstructions while replacing irregularities, therefore, acting as a filter for anomalous patterns. The prediction procedure is also very efficient as the whole image is processed in one single step - unlike related ideas based on the sliding window approach [3], [16].

There is one potential problem with the above approach due to anomaly score being defined by the reconstruction error which is sensitive to the variation of pixel intensities in the following sense. On the one hand, a high variation in pixel intensities (e. g. pepper noise) in the normal regions is likely to result in false positive detections. On the other hand, anomalous regions with a strong structural difference might not be detected if the color distribution of the

corresponding pixels is close to the one of normal data resulting in a small reconstruction error. To address this issue we modify the training objective such that the network is penalised for producing a high reconstruction error in the normal regions while being rewarded for a higher reconstruction error in the distorted areas. The resulting network shows a kind of hybrid behaviour. On the one hand it aims at reconstructing the normal regions and on the other hand it amplifies the reconstruction error for the anomalous regions by further disturbing the corresponding area acting almost as a segmentation network. Altogether, the proposed approach allows for an accurate localisation of the anomalous regions as we demonstrate in the experimental section.

The rest of the paper is organised as follows. In Section 2 we first discuss the main differences of our idea with respect to the related works. In Section 3 we formally introduce the proposed framework including the training procedure and the model architecture. In Section 4 we evaluate the performance of our approach and provide the experimental results based on the publicly available MVTec AD dataset [24], [25] for the task of visual anomaly detection. We finish our discussion with a conclusion in Section 5.

2 RELATED WORKS

In the context of automatic surface inspection, [3] proposed an anomaly detection approach based on neural image completion. Specifically, they train a convolutional neural network (CNN) to reconstruct small image patches for which a rectangular center area has been cut out. Using sliding window approach during prediction phase they compute a reconstruction error on the whole input image. To be able to complete the central region, a model must learn meaningful features which allow to interpolate the local context. Although presenting an inspiring idea, this approach has two significant issues. First, cutting out an area prevents reconstruction of locally confined patterns which cannot be computed from the context. Regardless if a corresponding pattern is anomalous or normal, it will be lost during the completion process resulting in a high reconstruction error. Second, the presented idea relies on a sliding window approach to detect anomalies at different image locations resulting in a slower inference during prediction phase. In contrast, we process the whole input image in one single step. Furthermore, our training objective does not rely on reconstruction of missing patches but rather aims at reproducing normal regions within the input image and either filtering anomalous patterns or enlarging the reconstruction difference for the areas which are inconsistent with their surrounding context. In particular, no information about the image is lost during the prediction phase allowing for an accurate reconstruction of the anomaly-free regions which in turn improves the actual detection performance.

Another previous work [5] aims at preventing reconstruction of anomalous patterns by projecting the inputs to the normal regions in the latent space. The training and prediction phase are performed in two steps. Specifically, the authors first adopt a variational autoencoder as the reconstruction model to get a discrete latent space of normal samples. Then a deep autoregressive model is used to estimate the probability model of the discrete latent space.

In the detection stage this autoregressive model is used to determine which parts of the signal deviate from the data distribution in the latent space and should be resampled to yield a restored image which is closest to the anomaly input. In contrast, our approach requires a single inference pass in both phases and requires no additional resampling.

More recent works [16], [26] also rely on the idea of image inpainting originally introduced in [3]. The work in [26] replaces the sliding window procedure by a different approach. First the input image is divided in a grid of cells and a number of images is created by randomly removing some cells in the original image. Inference is then performed on each single image and the resulting reconstruction is assembled from partial reconstructions of all images. The method in [16] further rely on the sliding window idea, but unlike other methods use a self-attention based transformer instead of convolutional autoencoders. According to the authors one small drawback of the their approach is increased training times due to transformer architecture. Both methods achieve very accurate results on the MVTec AD dataset [24], [25].

Another method proposed in [15], is similar to our idea in the sense that it also modifies input images to artificially create anomalous regions using a specific Cut&Paste augmentation technique. Unlike our method, however, it is a two-stage approach relying on training an additional binary classifier for detection and localisation of the anomalous regions based on the GradCAM [27] visual explanation algorithm.

3 METHODOLOGY

In this section we introduce a self-supervised framework for training autoencoders to detect anomalies in images. We describe the objective function, the data generation process during training, and our choice of model architecture.

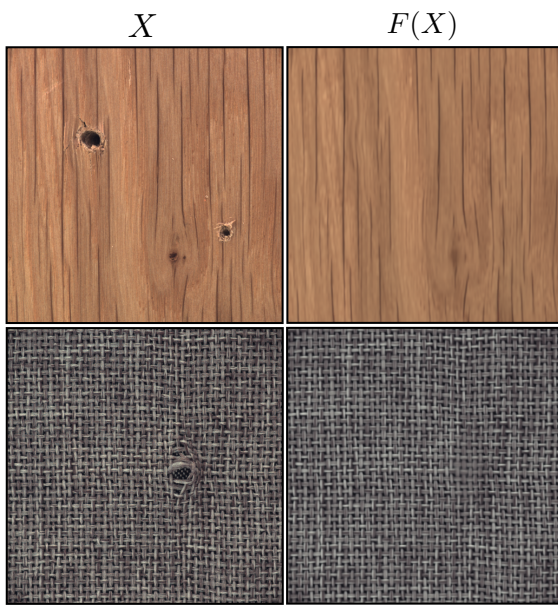


Fig. 2. Illustration of the reconstruction effect of two models trained either on the wooden or carpet surface images (without defects) from the MVTec AD dataset using objective (1).

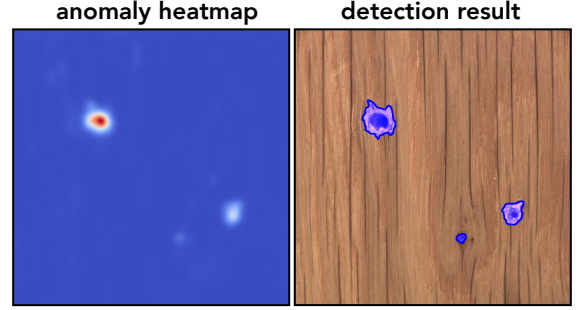


Fig. 3. Illustration of how anomaly detection is performed by thresholding a computed anomaly heatmap for the wooden example in Fig. 2.

3.1 Training Objective

We use $F: [0, 1]^{n \times m \times 3} \rightarrow [0, 1]^{n \times m \times 3}$, $n, m \in \mathbb{N}$ to denote a mapping related to a neural network that implements an autoencoder with input and output tensors corresponding to color images. Furthermore, we denote by $X \in [0, 1]^{n \times m \times 3}$ an original image and by \hat{X} a copy of X which has been partially modified. The modified regions within \hat{X} are marked by a binary mask $M \in \{0, 1\}^{n \times m \times 3}$, where \bar{M} denotes a corresponding complement. Given this notation, our training objective can be written as follows:

$$\mathcal{L}(\hat{X}, X) = \frac{\lambda}{\|\bar{M}\|_1} \cdot \|\bar{M} \odot (F(\hat{X}) - X)\|_2 + \frac{(1 - \lambda)}{\|M\|_1} \cdot \|M \odot (F(\hat{X}) - X)\|_2 \quad (1)$$

where \odot denotes an element-wise tensor multiplication and $\lambda \in [0, 1]$ is a weighting parameter for controlling the importance of the two terms during training. $\|\cdot\|_p$ for $p \in \mathbb{N}_+$ denotes the L^p -norm on a corresponding tensor space. In terms of supervised learning, we feed a partially modified image \hat{X} as input to the network aiming to reconstruct the original ground truth image X representing the label.

By minimising the above objective, a corresponding autoencoder aims at learning to perform two tasks. The first term pushes the network towards an accurate reconstruction of the masked input image $\bar{M} \odot X$ from a latent space, while the second term requires the network to correct the modified regions $M \odot \hat{X}$ by restoring the original image. Altogether, the objective in equation (1) steers the behaviour of a corresponding autoencoder to produce locally consistent reconstructions while replacing irregularities, acting in some sense as a filter for anomalous patterns. Figure 2 shows some reconstruction examples from two models trained either on wooden or carpet surface images from the MVTec AD dataset without defects [24]. We can see how normal regions are replicated by the model while irregularities (e.g., holes) are replaced by locally consistent patterns.

Given a trained autoencoder F and an input image X , anomaly detection can be performed by thresholding a corresponding anomaly heatmap computed by averaging the term $\|F(X) - X\|_2$ over the color channels as illustrated in Fig. 3. To get a more robust result we smooth the anomaly heatmap using a gaussian filter before thresholding.

In some cases, autoencoders trained using objective (1) can fail to produce accurate detection results. As already

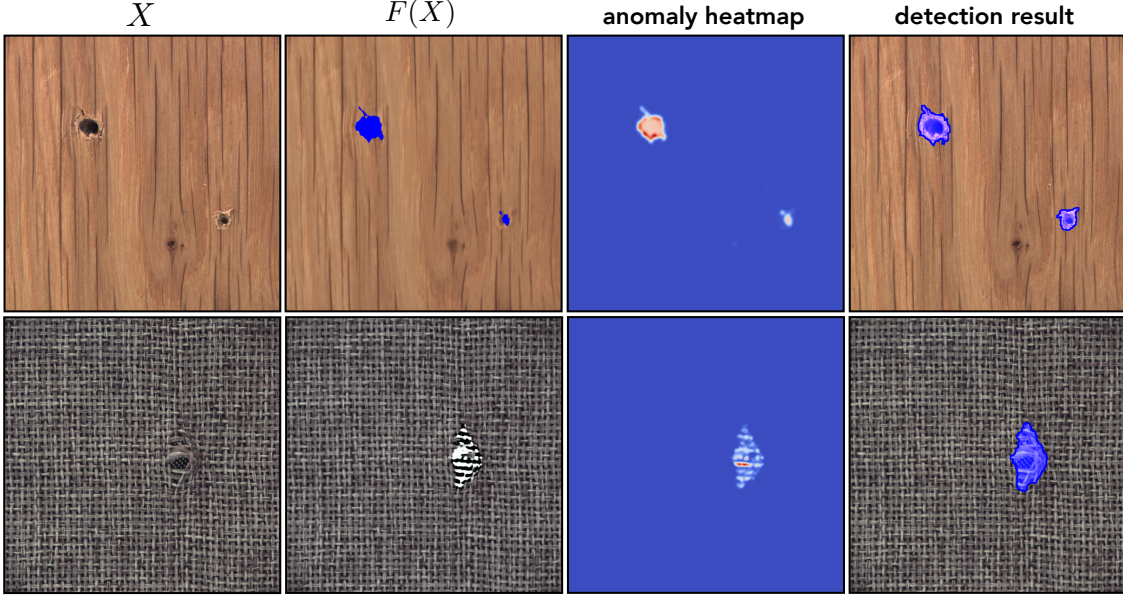


Fig. 4. Illustration of the reconstruction and detection effect of two models trained either on the wooden or carpet surface images (without defects) from the MVTec AD dataset using objective (2).

mentioned in the introduction, a problem with the above approach is that the reconstruction error is sensitive to the pixel intensities. Anomalous regions even with a strong structural deviation from normal patterns but of low contrast might not be detected, if the reconstruction $F(X)$ has similar pixel intensities as the input X (see Fig. ?? for an example). Therefore, we adjust our training objective in (1) to reward a higher reconstruction error in the distorted areas as follows:

$$\begin{aligned} \mathcal{L}(\hat{X}, X) = & \frac{\lambda}{\|\bar{M}\|_1} \cdot \left\| \bar{M} \odot (F(\hat{X}) - X) \right\|_2 - \\ & \frac{(1 - \lambda)}{\|M\|_1} \cdot \left\| M \odot (F(\hat{X}) - X) \right\|_2 \end{aligned} \quad (2)$$

Note the minus sign between the two terms in the objective. The first term encourages the network to produce an accurate reconstruction of the normal regions while the second term amplifies the reconstruction error for the anomalous regions increasing the contrast in the resulting anomaly heatmap. Figure 4 illustrates some reconstruction and detection results when trained using objective (2). Note how the anomalous regions are emphasised in the reconstruction $F(\hat{X})$ resembling, in some sense, the performance of a model trained for the task of semantic segmentation. Namely, the anomalous regions in the wooden example are emphasised by the blue color while the color of the anomalous pixels in the carpet example is alternating between black and white resulting in a high reconstruction error. In order to decrease the loss value the network also has to put more attention on the task of localising anomalous regions potentially improving the final localisation performance. In the case where anomalies have a low contrast in the surrounding neighbourhood this improvement can be very dramatic as we show in the experimental section. Figure 6 provides some examples illustrating the qualitative difference between the two objectives in such a case.

There is one final adjustment we need to make to prevent the following unwanted effect. Depending on the type of transformation applied to X to get \hat{X} , the objective (2) can put too much weight on the second term. Namely, the loss can be easily decreased by setting the pixel values $F(\hat{X})$ within the mask M to achieve maximal difference to the corresponding pixels in X completely ignoring the actual pixel difference $|\hat{X} - X|$. In particular, if some regions have exactly the same pixel values in both images, the objective (2) still encourages the network to increase the reconstruction error for these regions. We tackle this by replacing the binary mask M with a real-valued mask $|\hat{X} - X| \in [0, 1]^{n \times m \times 3}$, therefore, reducing the importance of the second term according to the relative pixel difference. Our final objective is given as follows:

$$\begin{aligned} \mathcal{L}(\hat{X}, X) = & \frac{\lambda}{\|\bar{M}\|_1} \cdot \left\| \bar{M} \odot (F(\hat{X}) - X) \right\|_2 - \\ & \frac{(1 - \lambda)}{\|\hat{X} - X\|_1} \cdot \left\| |\hat{X} - X| \odot (F(\hat{X}) - X) \right\|_2 \end{aligned} \quad (3)$$

We note that our image modification procedure ensures that inequality $\|\hat{X} - X\|_1 > 0$ always holds.

3.2 Data Generation and Training

Since we use a self-supervised approach we need to provide a training data consisting of input-output pairs. The ground truth outputs are given by the original images from the normal data. The inputs are generated from these images by partially modifying some regions as follows. In the first step we randomly sample size and location of a patch to be modified. Then a corresponding patch is extracted and passed through an elastic deformation process. Additionally, we randomly define a shape mask to mask the content of the patch. In the last step the shape mask is embedded in a two-dimensional zero-array to define a global mask M . Finally, a corresponding content of the original image X

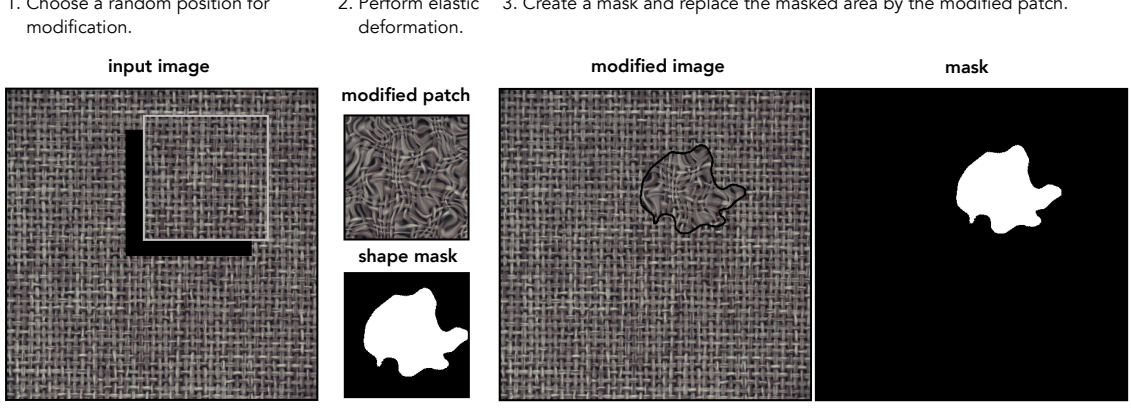


Fig. 5. Illustration of the label generation process during training. In the first step we randomly choose the size and location of a patch to be modified. In the second step a corresponding patch is extracted and transformed using elastic deformation. Also a shape mask is created for the content of the transformed patch. In the last step the shape mask is embedded into an empty image to define a global mask M and a corresponding content of the original image X is replaced by the masked modified patch giving modified image \hat{X} .

is replaced by the masked modified patch giving modified image \hat{X} . The whole procedure is illustrated in Fig. 5. Note that the dark line marking the borders of the modification (in step 3) is only for illustration purposes and is not present in the training data.

During training we sample images from the ground truth data representing the outputs from which we generate distorted inputs to be passed to the network. We experimented with different transformations of the original images like simple cut-out, patch swapping and elastic deformation with the latter providing the best results. We also found that it can be useful (depending on the data) to vary the brightness of modified patches. Furthermore, we use a progressive training scheme gradually increasing the size of the input images over the course of the training phase. During testing phase there is no input modification and images are passed unchanged to the network. Anomalous regions are then detected by thresholding a corresponding heatmap computed from the difference between the inputs and the outputs produced by the autoencoder.

3.3 Model

We follow an established architecture of deep autoencoders, where the encoder is build from layers gradually decreasing spatial dimension and increasing the number of feature maps while the decoder reverses this process by increasing the spatial dimension and decreasing the number of channels. An important detail here is that additionally to the standard convolutions we exploit the dilated convolutions for approximating higher order dependencies between the individual pixels and their local neighbourhood. An overview of the whole architecture is given in Table 1.

Here, after each convolution *Conv.* (except in the last layer) we use batch normalisation and rectified linear units (ReLU) as the activation function. Max-pooling *MaxPool.* is applied to reduce the spatial dimension of the intermediate feature maps. *Transp. Conv.* denotes the convolution transpose operation and also uses batch normalisation with ReLUs. In the last layer we use a sigmoid activation function without batch normalisation. We observed that using batch normalisation in the last layer sometimes can lead to strong

gridding effects in the reconstruction. $SDC_{1,2,4,8,16}$ refers to a stacked dilated convolution where multiple dilated convolutions are stacked together. The corresponding subscript $\{1, 2, 4, 8, 16\}$ denotes the dilation rates of the five individual convolutions in each stack.

TABLE 1
Model architecture.

Layer Type	Number of Filters	Filter Size	Output Size
Conv.	32	3×3	$512 \times 512 \times 32$
Conv.	32	3×3	$512 \times 512 \times 32$
MaxPool.		$2 \times 2 / 2$	$256 \times 256 \times 32$
Conv.	64	3×3	$256 \times 256 \times 64$
Conv.	64	3×3	$256 \times 256 \times 64$
MaxPool.		$2 \times 2 / 2$	$128 \times 128 \times 64$
Conv.	128	3×3	$128 \times 128 \times 128$
Conv.	128	3×3	$128 \times 128 \times 128$
MaxPool.		$2 \times 2 / 2$	$64 \times 64 \times 128$
$SDC_{1,2,4,8,16}$	64×5	5×5	$64 \times 64 \times 320$
$SDC_{1,2,4,8,16}$	64×5	5×5	$64 \times 64 \times 320$
$SDC_{1,2,4,8,16}$	64×5	5×5	$64 \times 64 \times 320$
$SDC_{1,2,4,8,16}$	64×5	5×5	$64 \times 64 \times 320$
Conv.	256	3×3	$64 \times 64 \times 256$
Transp. Conv.	256	$3 \times 3 / 2$	$128 \times 128 \times 256$
Conv.	256	3×3	$128 \times 128 \times 256$
Conv.	128	3×3	$128 \times 128 \times 128$
Transp. Conv.	128	$3 \times 3 / 2$	$256 \times 256 \times 128$
Conv.	128	3×3	$256 \times 256 \times 128$
Conv.	64	3×3	$256 \times 256 \times 64$
Transp. Conv.	64	$3 \times 3 / 2$	$512 \times 512 \times 64$
Conv.	64	3×3	$512 \times 512 \times 64$
Conv.	32	3×3	$512 \times 512 \times 32$
Conv.	3	1×1	$512 \times 512 \times 3$

4 EXPERIMENTAL ANALYSIS

In this section we evaluate the performance of our approach for the task of anomaly detection in images and compare the results with the existing baseline methods.

4.1 Data and Setup

We used the public MVTec Anomaly Detection dataset [24], [25] in our experiments consisting of 5 texture and 10 object categories. The texture categories cover both regular (carpet, grid) and random pattern cases (leather, tile, wood). This dataset has been widely used as a benchmark for anomaly detection and localisation in the manufacturing domain. To increase the amount of the training data we used simple data augmentation like rotation by a multiple of 90 degrees, as well as horizontal and vertical flipping depending on the category. For each category we trained a separate model presented in Table 1 by optimising either for objective (1) or (3).

4.2 Evaluation Metrics

To compare with the previous works we use the same evaluation setup defined in [24]. For each category we first set a threshold for the minimal area of connected components to be considered as an anomaly. Then we evaluate our trained model on the validation set containing normal images only and set a threshold for the anomaly score such that the area of the largest connected component in the computed anomaly heatmaps is slightly below defined minimum area. The final performance on the test data is then evaluated with respect to this threshold.

For the sake of comparison we compute metrics used in the previous works including true positives rate (TPR) and true negatives rate (TNR) according to

$$TPR = \frac{TP}{TP + FN}, \quad TNR = \frac{TN}{TN + FP} \quad (4)$$

where TP , TN , FP , FN denote the numbers of true positives, true negatives, false positives and false negatives, respectively. Additionally, we evaluate the performance of

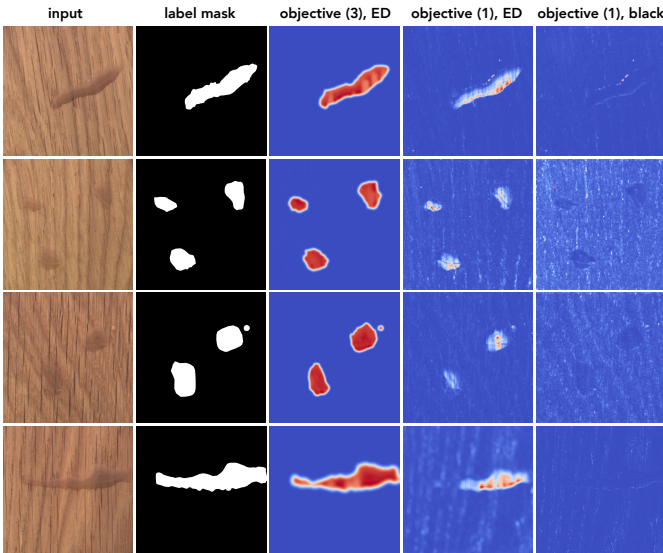


Fig. 6. Illustration of qualitative performance difference when training either with objective (3) (third column) or (1) (fourth and fifth column). The first two columns show the input images and the label masks. "ED" indicates that Elastic Deformation has been used for creating modified patches during training. "BLACK" indicates that modified area has been cut out by setting its pixel values to zeros.

our approach (on the image and pixel level) using F_1 score according to

$$F_1 = \frac{2 \cdot TP}{2 \cdot TP + FP + FN}. \quad (5)$$

For localisation, we additionally report the pixel-wise area under the ROC (AUROC) metric which is independent of the chosen threshold for anomaly score. In the case where we had access to the corresponding numbers, we additionally compare the performance of our approach to the previous methods in terms of F_1 measure on image-level and on pixel-level accumulated over the test set. Table 4 demonstrates the corresponding results.

4.3 Results

First we evaluate the recognition performance of our approach on the image-level by looking how well it can distinguish between normal and anomalous images. To compare to the previous works we evaluate the TPR and TNR and provide an average of the two in Table 2. To evaluate the localisation performance independently of the chosen threshold, we present in Table 3 the corresponding values for the AUROC metric. The values for the baseline models are directly taken from the corresponding publications. In the case where we had access to the corresponding numbers, we additionally compare the performance of our approach to the previous methods in terms of F_1 measure on image-level and on pixel-level accumulated over the test set. Note that these values are dependent on the chosen threshold for anomaly score. Table 4 shows the corresponding results.

To summarise, we can see that our approach (on average) provides more accurate results for both recognition and localisation of anomalous regions and consistently outperforms the previous methods for the texture categories. To give a sense of visual quality of the resulting segmentations we show a few examples in Figure 1 and further examples in Figure 7.

4.4 Discussion

We presented two different objectives (1) and (3) for training an autodecoder for the task of anomaly detection. For practical cases we can use either of the two to get an accurate model. However, there are some interesting differences which we discuss below.

Training with the objective (1) seems easier from the practical perspective. There is a good measure of training progress given by the reconstruction error which strongly correlates with the ability of the model to remove anomalous patterns from images. Therefore, the reconstruction error is a good approximation for our target loss in that case. Also the choice of a good value for the weighting parameter λ is rather straightforward - setting $\lambda = 0.5$ turns out to be sufficiently good. Using elastic deformation as a distortion technique pushes the model to act as a filter for anomalous patterns by replacing irregularities with locally consistent reconstructions. Therefore, the resulting model is capable of detecting a variety of anomalous patterns - even the ones being close to the data manifold.

The objective (3), is more similar to a segmentation network and can, therefore, provide more accurate results with

TABLE 2

Experimental results for recognition of anomalous images given as an **average of TPR and TNR** for texture categories of the MVTec AD dataset.

Category	AE _{SSIM} [4]	AE _{L2} [4]	AnoGAN [8]	CNNFD [9]	TI [10]	CAVGA-D _u [7]	LSR [5]	Ours
Carpet	0.67	0.50	0.49	0.63	0.59	0.73	0.71	0.99
Grid	0.69	0.78	0.51	0.67	0.50	0.75	0.91	1.0
Leather	0.46	0.44	0.52	0.67	0.50	0.71	0.96	1.0
Tile	0.52	0.77	0.51	0.71	0.72	0.70	0.95	0.99
Wood	0.83	0.74	0.68	0.84	0.71	0.85	0.96	1.0
avg. textures	0.63	0.65	0.54	0.70	0.60	0.75	0.90	0.99
Bottle	0.88	0.80	0.69	0.53	-	0.89	0.99	0.99
Cable	0.61	0.56	0.53	0.61	-	0.63	0.72	0.74
Capsule	0.61	0.62	0.58	0.41	-	0.83	0.68	0.83
Hazelnut	0.54	0.88	0.50	0.49	-	0.84	0.94	0.93
Metal Nut	0.54	0.73	0.50	0.65	-	0.67	0.83	0.63
Pill	0.60	0.62	0.62	0.46	-	0.88	0.68	0.86
Screw	0.51	0.69	0.35	0.43	-	0.77	0.80	0.86
Toothbrush	0.74	0.98	0.57	0.57	-	0.91	0.92	1.0
Transistor	0.52	0.71	0.67	0.58	-	0.73	0.73	0.92
Zipper	0.80	0.80	0.59	0.54	-	0.87	0.97	0.99
avg. objects	0.64	0.88	0.74	0.53	-	0.80	0.83	0.88
avg. all	0.63	0.82	0.71	0.59	-	0.78	0.85	0.92

TABLE 3

Experimental results for the anomaly segmentation task given as **AUROC** on each texture category of MVTec AD dataset.

Category	AE _{SSIM} [4]	AE _{L2} [4]	AnoGAN [8]	CNNFD [9]	VAE [11]	LSR [5]	CutPaste [15]	InTra [16]	Ours
Carpet	0.87	0.59	0.54	0.72	0.78	0.94	0.98	0.99	0.99
Grid	0.94	0.90	0.58	0.59	0.73	0.99	0.97	0.98	0.99
Leather	0.78	0.75	0.64	0.87	0.95	0.99	0.99	0.99	0.99
Tile	0.59	0.51	0.50	0.93	0.80	0.88	0.90	0.94	0.97
Wood	0.73	0.73	0.62	0.91	0.77	0.87	0.95	0.89	0.97
avg. textures	0.78	0.70	0.58	0.80	0.81	0.93	0.96	0.96	0.98
Bottle	0.93	0.86	0.86	0.78	0.87	0.95	0.98	0.97	0.95
Cable	0.82	0.86	0.86	0.78	0.87	0.95	0.90	0.91	0.96
Capsule	0.94	0.88	0.84	0.84	0.74	0.93	0.97	0.98	0.98
Hazelnut	0.97	0.95	0.87	0.72	0.98	0.95	0.97	0.98	0.98
Metal Nut	0.89	0.86	0.76	0.82	0.94	0.91	0.93	0.93	0.95
Pill	0.91	0.85	0.87	0.68	0.83	0.95	0.96	0.98	0.98
Screw	0.96	0.96	0.80	0.87	0.97	0.96	0.97	0.99	0.99
Toothbrush	0.92	0.93	0.90	0.77	0.94	0.97	0.98	0.99	0.98
Transistor	0.90	0.86	0.80	0.66	0.93	0.91	0.93	0.96	0.97
Zipper	0.88	0.77	0.78	0.76	0.78	0.98	0.99	0.99	0.99
avg. objects	0.91	0.88	0.83	0.77	0.89	0.95	0.96	0.97	0.97
avg. all	0.87	0.82	0.75	0.78	0.86	0.94	0.96	0.96	0.98

respect to the localisation performance. Unlike objective (2), however, objective (3) is more sensitive with respect to the type of distortions we use during training. Therefore, it is potentially more prone to overfitting and we must rely on early stopping to get accurate results. Also the search for good λ values is more difficult because the second term tends to influence the training in a less predictable way. Despite these difficulties the increase in the localisation performance can be very significant in comparison to objective (2) as we showed in Figure 6 for the case of glue drops on a wooden surface. As a future work we will investigate how the type of artificial anomalous patterns influences the training progress with respect to overfitting.

As a final remark we note that training a model in a supervised way by using a segmentation loss directly on the artificially generated anomalies does not provide good results. It begins to overfit on used distortion patterns

already after a few training epochs. For example, it quickly learns to localise the elastic distortions but completely fails to recognise real anomalies from the test set.

5 CONCLUSION

We presented a self-supervised learning framework for the task of visual anomaly detection by training deep convolutional autoencoders on partially distorted images (with one of two different objectives). Our approach allows to use discriminative information during training to better distinguish between normal and anomalous regions in the testing phase. A model trained via objective (1) acts, in some sense, as a filter for anomalous patterns by replacing irregularities with locally consistent reconstructions. Due to this fact, it is capable of detecting a variety of anomalous patterns - even the ones being close to the data manifold.

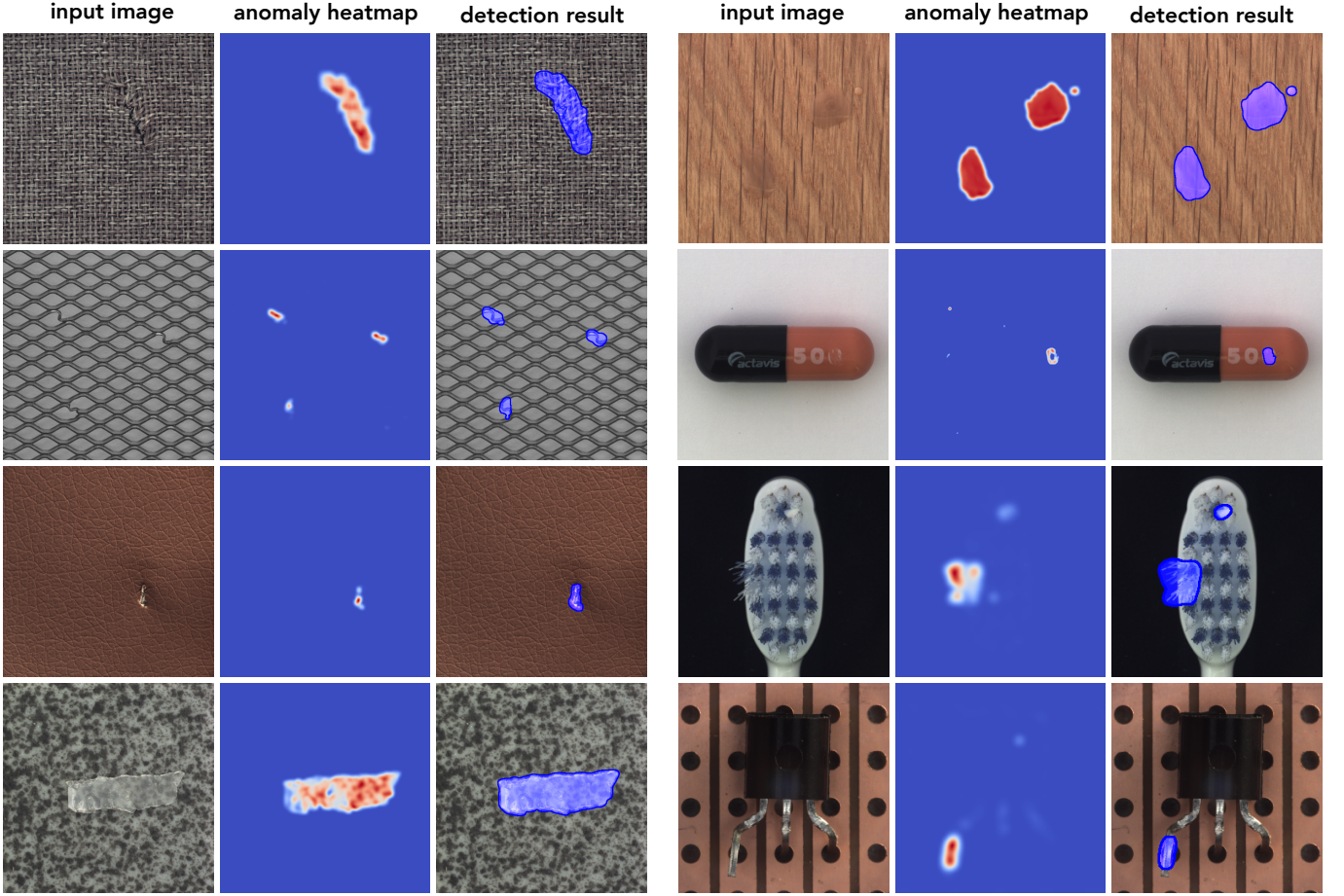


Fig. 7. Illustration of anomaly detection results when training according to the objective (3). The columns show the input images, the anomaly heatmaps, and the resulting segmentation masks for the anomalous regions.

TABLE 4

Experimental results for the anomaly detection task using **F₁ measure** on **image-level** (first number) and on **pixel-level** (second number) accumulated over the test set for each texture category of MVTec AD dataset.

Category	AE _{SSIM} [4]	AE _{L2} [4]	LSR [5]	Ours
Carpet	0.87/0.08	0.54/0.03	0.88/0.33	0.99/0.76
Grid	0.90/0.02	0.92/0.04	0.97/0.38	1.0/0.58
Leather	0.81/0.02	0.76/0.32	0.98/0.42	1.0/0.53
Tile	0.09/0.07	0.71/0.07	0.98/0.30	0.99/0.74
Wood	0.88/0.12	0.64/0.24	0.97/0.42	1.0/0.67
avg. textures	0.71/0.06	0.71/0.14	0.96/0.37	0.99/0.66
Bottle	0.92/0.16	0.90/0.26	0.99/0.55	0.99/0.62
Cable	0.58/0.02	0.29/0.06	0.82/0.40	0.85/0.54
Capsule	0.58/0.08	0.39/0.10	0.68/0.23	0.91/0.43
Hazelnut	0.13/0.44	0.89/0.46	0.93/0.50	0.95/0.59
Metal Nut	0.15/0.03	0.83/0.25	0.93/0.36	0.91/0.66
Pill	0.43/0.09	0.37/0.25	0.81/0.20	0.93/0.37
Screw	0.11/0.06	0.56/0.20	0.81/0.34	0.89/0.44
Toothbrush	0.80/0.14	0.98/0.35	0.97/0.40	1.0/0.53
Transistor	0.06/0.07	0.60/0.19	0.68/0.11	0.90/0.63
Zipper	0.75/0.29	0.77/0.15	0.99/0.58	0.99/0.80
avg. objects	0.45/0.14	0.66/0.23	0.86/0.37	0.93 / 0.56
avg. all	0.54 / 0.11	0.68 / 0.20	0.89 / 0.37	0.95 / 0.59

When training with objective (3) the resulting model, on the one hand, aims to reconstruct the normal regions resulting in a low reconstruction error and on the other hand it amplifies the reconstruction error for the anomalous regions acting almost as a segmentation network. This potentially allows to boost final localisation performance - as we showed in the experimental section in Figure 6. In contrast to the pure segmentation approach, however, the resulting model focuses on the data manifold preventing overfitting on specific patterns produced by a chosen transformation to create distorted inputs. Finally, the inference with our method (during training and prediction) is very efficient processing the whole input image in one single step - unlike related previous methods. In our experiments on the publicly available MVTec Anomaly Detection dataset we showed that the new approach achieves (on average) a higher recognition and localisation performance. On the texture-subset, in particular, it consistently outperforms a bunch of recent anomaly detection methods by a big margin.

REFERENCES

[1] B. Schölkopf, J. C. Platt, J. Shawe-Taylor, A. J. Smola, and R. C. Williamson, "Estimating the support of a high-dimensional distribution," *Neural Comput.*, vol. 13, no. 7, pp. 1443–1471, 2001.

[2] L. Ruff, N. Görnitz, L. Deecke, S. A. Siddiqui, R. A. Vandermeulen, A. Binder, E. Müller, and M. Kloft, "Deep one-class classification," in *Proceedings of the 35th International Conference on Machine Learning, ICML 2018, Stockholm, Sweden, July 10-15, 2018*, ser. Proceedings of Machine Learning Research, J. G. Dy and A. Krause, Eds., vol. 80. PMLR, 2018, pp. 4390-4399.

[3] M. Haselmann, D. P. Gruber, and P. Tabatabai, "Anomaly detection using deep learning based image completion," in *17th IEEE International Conference on Machine Learning and Applications, ICMLA 2018, Orlando, FL, USA, December 17-20, 2018*, M. A. Wani, M. M. Kantardzic, M. S. Mouchaweh, J. Gama, and E. Lughofer, Eds. IEEE, 2018, pp. 1237-1242.

[4] P. Bergmann, S. Löwe, M. Fauser, D. Sattlegger, and C. Steger, "Improving unsupervised defect segmentation by applying structural similarity to autoencoders," in *Proceedings of the 14th International Joint Conference on Computer Vision, Imaging and Computer Graphics Theory and Applications, VISIGRAPP 2019, Volume 5: VISAPP, Prague, Czech Republic, February 25-27, 2019*, A. Trémeau, G. M. Farinella, and J. Braz, Eds. SciTePress, 2019, pp. 372-380.

[5] L. Wang, D. Zhang, J. Guo, and Y. Han, "Image anomaly detection using normal data only by latent space resampling," *Applied Sciences*, vol. 10, no. 23, 2020.

[6] P. Bergmann, M. Fauser, D. Sattlegger, and C. Steger, "Uninformed students: Student-teacher anomaly detection with discriminative latent embeddings," in *2020 IEEE/CVF Conference on Computer Vision and Pattern Recognition, CVPR 2020, Seattle, WA, USA, June 13-19, 2020*. Computer Vision Foundation / IEEE, 2020, pp. 4182-4191.

[7] S. Venkataraman, K. Peng, R. V. Singh, and A. Mahalanobis, "Attention guided anomaly localization in images," in *Computer Vision - ECCV 2020 - 16th European Conference, Glasgow, UK, August 23-28, 2020, Proceedings, Part XVII*, ser. Lecture Notes in Computer Science, A. Vedaldi, H. Bischof, T. Brox, and J. Frahm, Eds., vol. 12362. Springer, 2020, pp. 485-503.

[8] T. Schlegl, P. Seeböck, S. M. Waldstein, U. Schmidt-Erfurth, and G. Langs, "Unsupervised anomaly detection with generative adversarial networks to guide marker discovery," in *Information Processing in Medical Imaging - 25th International Conference, IPMI 2017, Boone, NC, USA, June 25-30, 2017, Proceedings*, ser. Lecture Notes in Computer Science, M. Niethammer, M. Styner, S. R. Aylward, H. Zhu, I. Oguz, P. Yap, and D. Shen, Eds., vol. 10265. Springer, 2017, pp. 146-157.

[9] P. Napoletano, F. Piccoli, and R. Schettini, "Anomaly detection in nanofibrous materials by cnn-based self-similarity," *Sensors*, vol. 18, no. 1, p. 209, 2018.

[10] T. Böttger and M. Ulrich, "Real-time texture error detection on textured surfaces with compressed sensing," *Pattern Recognit. Image Anal.*, vol. 26, pp. 88-94, 2016.

[11] W. Liu, R. Li, M. Zheng, S. Karanam, Z. Wu, B. Bhanu, R. J. Radke, and O. I. Camps, "Towards visually explaining variational autoencoders," in *2020 IEEE/CVF Conference on Computer Vision and Pattern Recognition, CVPR 2020, Seattle, WA, USA, June 13-19, 2020*. IEEE, 2020, pp. 8639-8648.

[12] D. M. J. Tax and R. P. W. Duin, "Support vector data description," *Mach. Learn.*, vol. 54, no. 1, pp. 45-66, 2004.

[13] P. Chong, L. Ruff, M. Kloft, and A. Binder, "Simple and effective prevention of mode collapse in deep one-class classification," in *2020 International Joint Conference on Neural Networks, IJCNN 2020, Glasgow, United Kingdom, July 19-24, 2020*. IEEE, 2020, pp. 1-9.

[14] C. Hu, Y. Feng, H. Kamigaito, H. Takamura, and M. Okumura, "One-class text classification with multi-modal deep support vector data description," in *Proceedings of the 16th Conference of the European Chapter of the Association for Computational Linguistics: Main Volume, EACL 2021, Online, April 19 - 23, 2021*, P. Merlo, J. Tiedemann, and R. Tsarfaty, Eds. Association for Computational Linguistics, 2021, pp. 3378-3390.

[15] C. Li, K. Sohn, J. Yoon, and T. Pfister, "Cutpaste: Self-supervised learning for anomaly detection and localization," in *IEEE Conference on Computer Vision and Pattern Recognition, CVPR 2021, virtual, June 19-25, 2021*. Computer Vision Foundation / IEEE, 2021, pp. 9664-9674.

[16] J. Pirnay and K. Chai, "Inpainting transformer for anomaly detection," in *Image Analysis and Processing - ICIAP 2022 - 21st International Conference, Lecce, Italy, May 23-27, 2022, Proceedings, Part II*, ser. Lecture Notes in Computer Science, S. Sclaroff, C. Distante, M. Leo, G. M. Farinella, and F. Tombari, Eds., vol. 13232. Springer, 2022, pp. 394-406.

[17] P. Vincent, H. Larochelle, Y. Bengio, and P. Manzagol, "Extracting and composing robust features with denoising autoencoders," in *Machine Learning, Proceedings of the Twenty-Fifth International Conference (ICML 2008), Helsinki, Finland, June 5-9, 2008*, ser. ACM International Conference Proceeding Series, W. W. Cohen, A. McCallum, and S. T. Roweis, Eds., vol. 307. ACM, 2008, pp. 1096-1103.

[18] J. Deng, Z. Zhang, E. Marchi, and B. W. Schuller, "Sparse autoencoder-based feature transfer learning for speech emotion recognition," in *2013 Humaine Association Conference on Affective Computing and Intelligent Interaction, ACII 2013, Geneva, Switzerland, September 2-5, 2013*. IEEE Computer Society, 2013, pp. 511-516.

[19] D. Pathak, P. Krähenbühl, J. Donahue, T. Darrell, and A. A. Efros, "Context encoders: Feature learning by inpainting," in *2016 IEEE Conference on Computer Vision and Pattern Recognition, CVPR 2016, Las Vegas, NV, USA, June 27-30, 2016*. IEEE Computer Society, 2016, pp. 2536-2544.

[20] S. Iizuka, E. Simo-Serra, and H. Ishikawa, "Globally and locally consistent image completion," *ACM Trans. Graph.*, vol. 36, no. 4, pp. 107:1-107:14, 2017.

[21] J. Yu, Z. Lin, J. Yang, X. Shen, X. Lu, and T. S. Huang, "Generative image inpainting with contextual attention," in *2018 IEEE Conference on Computer Vision and Pattern Recognition, CVPR 2018, Salt Lake City, UT, USA, June 18-22, 2018*. IEEE Computer Society, 2018, pp. 5505-5514.

[22] G. Liu, F. A. Reda, K. J. Shih, T. Wang, A. Tao, and B. Catanzaro, "Image inpainting for irregular holes using partial convolutions," in *Computer Vision - ECCV 2018 - 15th European Conference, Munich, Germany, September 8-14, 2018, Proceedings, Part XI*, ser. Lecture Notes in Computer Science, V. Ferrari, M. Hebert, C. Sminchisescu, and Y. Weiss, Eds., vol. 11215. Springer, 2018, pp. 89-105.

[23] J. Yu, Z. Lin, J. Yang, X. Shen, X. Lu, and T. S. Huang, "Free-form image inpainting with gated convolution," in *2019 IEEE/CVF International Conference on Computer Vision, ICCV 2019, Seoul, Korea (South), October 27 - November 2, 2019*. IEEE, 2019, pp. 4470-4479.

[24] P. Bergmann, M. Fauser, D. Sattlegger, and C. Steger, "Mvtec AD - A comprehensive real-world dataset for unsupervised anomaly detection," in *IEEE Conference on Computer Vision and Pattern Recognition, CVPR 2019, Long Beach, CA, USA, June 16-20, 2019*. Computer Vision Foundation / IEEE, 2019, pp. 9592-9600.

[25] P. Bergmann, K. Batzner, M. Fauser, D. Sattlegger, and C. Steger, "The mvtec anomaly detection dataset: A comprehensive real-world dataset for unsupervised anomaly detection," *Int. J. Comput. Vis.*, vol. 129, no. 4, pp. 1038-1059, 2021.

[26] V. Zavrtanik, M. Kristan, and D. Skocaj, "Reconstruction by inpainting for visual anomaly detection," *Pattern Recognit.*, vol. 112, p. 107706, 2021.

[27] R. R. Selvaraju, M. Cogswell, A. Das, R. Vedantam, D. Parikh, and D. Batra, "Grad-cam: Visual explanations from deep networks via gradient-based localization," *Int. J. Comput. Vis.*, vol. 128, no. 2, pp. 336-359, 2020.